

A PROJECTION METHOD FOR PARTICLE RESAMPLING

MARK F. ADAMS*, DANIEL S. FINN†, MATTHEW G. KNEPLEY‡, AND JOSEPH V. PUSZTAY†

Abstract.

Particle discretizations of partial differential equations are advantageous for high-dimensional kinetic models in phase space due to their better scalability than continuum approaches with respect to dimension. Complex processes collectively referred to as *particle noise* hamper long time simulations with particle methods. One approach to address this problem is particle mesh adaptivity or remapping, known as *particle resampling*. This paper introduces a resampling method that projects particles to and from a (finite element) function space. The method is simple; using standard sparse linear algebra and finite element techniques, it can adapt to almost any set of new particle locations and preserves all moments up to the order of polynomial represented exactly by the continuum function space.

This work is motivated by the Vlasov-Maxwell-Landau model of magnetized plasmas with up to six dimensions, $3X$ in physical space and $3V$ in velocity space, and is developed in the context of a $1X + 1V$ Vlasov-Poisson model of Landau damping with logically regular particle and continuum phase space grids. [Stable long time dynamics are demonstrated up to \$T = 500\$ and reproducibility artifacts and data with stable dynamics up to \$T = 1000\$ is publicly available.](#)

Keywords: particle resampling, particle remapping, kinetic methods

1. Background. Particle, marker particle, or macro-particle methods, such as particle-in-cell (PIC), are discretizations that, akin to traditional continuum-based methods such as finite elements (FE), finite volume, etc., discretize continuous PDE models as opposed to discrete, ground truth models like molecular dynamics. Particle methods scale with dimension with a theoretical accuracy of $\mathcal{O}(N^{-\frac{1}{2}})$ and complexity $\mathcal{O}(N)$, with N particles, whereas continuum methods have higher order accuracy, $\mathcal{O}(N^{-p})$ for some order p , usually two or higher, the complexity is order $\mathcal{O}(N^D)$ with N grid points in each dimension D . For example, with a commonly attainable $p = 2$ the complexities cross over at $D = 4$ and particle methods have lower order complexity at higher dimensions. This scaling with dimension has motivated the use of the PIC methods for the Vlasov-Maxwell-Landau (VML) system, or Boltzmann’s equation with Coulomb collisions in Landau form for magnetized plasmas and Vlasov-Poisson-Landau in astrophysics [4].

Mesh or grid adaptivity is a fundamental tool in PDE modeling for both continuum and particle grid methods. Particle adaptivity, known as *particle resampling* in the physics community. This paper develops a particle resampling approach that uses a conservative mapping between particles and continuum grids, a projection [36], that conserves an arbitrary number of moments exactly, that was developed by the structure preserving discretization community for analysis purposes [22, 44]. This method allows for remapping a particle distribution to any new set of particles, supporting adaptivity in both the continuum grid construction and the particle grid definition. The focus of this paper is investigating the use of this projection for particle resampling with static regular grids for both particles and the finite element space with a standard plasma model problem. The testing codes are built on PETSc (Portable, Extensible Toolkit for Scientific Computation), and are publicly available (Appendix §A).

Particle resampling methods have been developed by many groups. Lapenta developed a method in the 1990s with a solve of the form, $(M_p M_p^T)^{-1}$, with Lagrange multipliers that enforce moment constraints explicitly [26, 25, 27], that is formally similar to the pseudoinverse solve in our approach §2.2. Colella et al., developed a *particle remapping* method that is similar to our approach in a finite volume context with a *direct remap* from the grid back to particles [43, 32, 33]. Faghihi et al. developed resampling methods with moment constraints and linear programming to enforce moments and other algebraic constraints [12]. Gonoskov proposed probabilistic down-sampling algorithms using algebraic constraints to enforced conservation [15]. Pfeiffer et al. introduced two conservative particle split and merge methods that use statistical properties of the plasma such as thermal speed [34]. Several groups have presented particle coalescence and splitting schemes, often using trees, on small groups of locally binned particles [39, 42, 5, 45, 28].

Our approach is distinguished from previous work in a few ways. An arbitrary number of moments are implicitly and provably conserved exactly without resorting to explicitly constraining the solution to desired manifolds. Our method is simple and built entirely on standard sparse linear algebra primitives and allows for almost any new distribution of particles, the original particle grid being a good choice if

*Lawrence Berkeley National Laboratory, Berkeley, CA (mfadams@lbl.gov)

†National Research Council Naval Research Laboratory Postdoctoral Fellow

‡University of Buffalo, Buffalo, NY

dynamic adaptivity is not desired. The Colella et al. algorithm is also flexible with phase-space adaptive mesh refinement (AMR) and is similar to our algorithm if the resampling set is chosen to align with the vertex points of the grid ($M_p = I$ in §2.1) [33], which results in the key component of this projection method, the pseudoinverse, vanishing.

This paper proceeds with relevant background in structure preserving methods in §2, the projection based resampling method in §3, numerical methods and the test problem in §4, §5 experiments with a direct remap method. Experiments with the full high-order finite element projection and remapping method are presented in §6, §7 investigates long time behavior with convergence studies, §8 discusses side effects of resampling, and §9 concludes with a discussion of potential future work.

2. Structure preserving methods for Boltzmann's equations. The critical idea in this work comes from research on structure preserving methods for Boltzmann's equations in general and the VML system for magnetized plasmas in particular, that results in a simple and elegant algorithm that provably conserves an arbitrary number of moments.

Hamiltonian models in phase space where density is a function of both space (\mathbf{x}) and velocity or momentum space (\mathbf{v}) are the fundamental equation of gravitational dynamics and electrostatics plasmas with the Vlasov-Poisson system, and electromagnetic plasmas with the Vlasov-Maxwell system. A Coulomb collision term accounts for the statistics of particle interactions not present in the Hamiltonian [16, 18, 3, 41, 20], giving rise to the governing equations for magnetized plasmas where the density of each species α is evolved in phase space according to

$$\frac{df_\alpha}{dt} \equiv \frac{\partial f_\alpha}{\partial t} + \frac{\partial \vec{x}}{\partial t} \cdot \nabla_{\mathbf{x}} f_\alpha + \frac{\partial \vec{v}}{\partial t} \cdot \nabla_{\mathbf{v}} f_\alpha = \sum_{\beta} C[f_\alpha, f_\beta]_{\alpha\beta},$$

where the collisional term is summed over all species β . This equation is composed of the symplectic *Vlasov-Maxwell* term $\frac{df}{dt} = 0$ and a metric, or diffusive, collision operator C , and Maxwells's equations provide an expression for $\frac{\partial \vec{v}}{\partial t} = a = \frac{q_\alpha}{m_\alpha} (\mathbf{E} + \mathbf{v} \times \mathbf{B})$.

This system has rich mathematical structure that can be preserved with proper discretizations. The metriplectic formalism is an approach to analyze VML and to develop *structure preserving* discretizations for the VML system [18, 22, 17]. When a structure preserving grid-based collision operator [18, 2, 1, 3] is coupled with a PIC method, a mechanism is needed to map distribution functions, in velocity space, between a particle representation and a finite element basis representation of the distribution function that preserves moments, as well as other structure [36]. Preserving the second moment in velocity space, energy, is critical for many applications.

2.1. Structure preserving particle-finite element basis mapping. To apply a continuum operator in a PIC method that conserves moments a conservative particle-finite element basis mapping and remapping method is required. Given a particle with weight w_p and position \mathbf{x}_p , a delta function representation $f_p(\mathbf{x}) = w_p \delta(\mathbf{x} - \mathbf{x}_p)$, and a finite element (FE) space V of functions ϕ_i and coefficients ρ_i , a function can be expressed as $f_{FE}(\mathbf{x}) = \sum_i \rho_i \phi_i(\mathbf{x})$. Ideally $f_{FE}(\mathbf{x}) = f_p(\mathbf{x})$, but that not possible. Weak equivalence can however be enforced with:

$$(2.1) \quad \int_{\Omega} d\mathbf{x} \phi_j(\mathbf{x}) \sum_p f_p(\mathbf{x}) = \int_{\Omega} d\mathbf{x} \phi_j(\mathbf{x}) \sum_p w_p \delta(\mathbf{x} - \mathbf{x}_p) = \int_{\Omega} d\mathbf{x} \phi_j(\mathbf{x}) f_{FE}(\mathbf{x}) = \int_{\Omega} d\mathbf{x} \phi_j(\mathbf{x}) \sum_i \rho_i \phi_i(\mathbf{x}) \forall \phi_j \in V.$$

With a *particle mass matrix* $M_p[i, j] \equiv \phi_i(\mathbf{x}_j)$, an FE mass matrix $M[i, j] \equiv \int_{\Omega} d\mathbf{x} \phi_i(\mathbf{x}) \phi_j(\mathbf{x})$, a vector of particle weights w and vector of FE weights ρ , (2.1) can be written in matrix form as

$$M\rho = M_p w,$$

which defines an equation for particle deposition:

$$(2.2) \quad \rho \leftarrow M^{-1} M_p w.$$

This mapping is proven to conserve moments up to the order polynomial that the FE space can represent exactly [19, 36], for example a quadratic element mesh is sufficient to conserve energy in velocity space.

After deposition on the FE space, a Poisson or Ampere's law solve can be executed or a collision operator, L , can be evolved, $u \leftarrow L\rho$. In mapping u back to particles one can simply invert (2.2), $\bar{w} \leftarrow M_p^{-1}Mu$, however M_p is rectangular in general. The key idea is that a pseudoinverse, M_p^\dagger with $M_p M_p^\dagger = I$, conserves moments:

$$(2.3) \quad \bar{w} \leftarrow M_p^\dagger M u.$$

Thus, if the collision operator conserves moments this entire process of applying a continuum operator in a PIC method conserves moments [18].

2.2. Pseudoinverses and idempotent projections. There are two basic approaches to the pseudoinverse: an appropriate Krylov methods such as LSQR or Moore-Penrose. Both of these solvers are l_2 projections, but there are alternative norms such as L_2 that could be investigated. Moore-Penrose is attractive because it is easier to precondition a square matrix, especially for batch solvers [3]. Krylov methods are attractive as they can solve singular systems transparently. Preconditioning LSQR requires some effort, but the pseudoinverse solves in this work are very well conditioned and unpreconditioned LSQR works well. Though we use LSQR in this work, the analysis is clearer with the Moore-Penrose pseudoinverse §3.1 because it is defined with standard matrix inverse: $M_p^\dagger \equiv M_p^T (M_p M_p^T)^{-1}$, and stability is easier to understand.

If a collision operator is not used, $L = I$, then combining (2.2) and (2.3) results in the remapping algorithm

$$(2.4) \quad \bar{w} \leftarrow M_p^T (M_p M_p^T)^{-1} M_p w,$$

which is a type of “coarse-graining” algorithm, a mechanism to add numerical entropy dissipation [8, 40].

Idempotent property of projections. Information is lost while projecting a particle representation of a function onto a FE basis if the number of particles exceeds the number of FE basis functions, which is the case of interest. An attractive property of (2.4) is that information is only lost on the first application in that

$$\bar{\bar{w}} = M_p^T (M_p M_p^T)^{-1} M_p \bar{w} = M_p^T (M_p M_p^T)^{-1} M_p M_p^T (M_p M_p^T)^{-1} M_p w = M_p^T (M_p M_p^T)^{-1} M_p w = \bar{w}.$$

Thus $\bar{\bar{w}} = \bar{w}$ and the coarse-graining operator is idempotent, which is an elegant property in that this process does not, in a sense, evolve the operator although it does add diffusion.

3. A particle resampling method. The key observation is that after computing (2.2), the distribution function is entirely represented on the FE space and particle weights and positions are no longer needed. A new set of particle positions, essentially any new set, can be created. A new particle mass matrix, \bar{M}_p , can then be computed and (2.4) can be continued with \bar{M}_p . Moments are conserved because it is provable, and experimentally demonstrated, that the projection to the grid preserves moments and the projection from the grid preserves moments. The framework for this resampling method is to rearrange (2.4), by projecting back to a new set of particles after the deposition according to:

- use (2.2) to deposit the distribution function on to the FE grid $c \leftarrow M_p w$,
- create a new set of particles to generate a new particle mass matrix \bar{M}_p ,
- apply a pseudoinverse to compute weights for the new particles $\bar{w} \leftarrow \bar{M}_p^\dagger c$.

Field preservation with resampling: $\bar{\rho} = \rho$. An attractive property of this resampling is that the right hand side of the field solves, Poisson and Ampere's law solves, or collision operators are not affected by the resampling:

$$\bar{\rho} = M^{-1} \bar{M}_p \bar{w} = M^{-1} \bar{M}_p \bar{M}_p^T (\bar{M}_p \bar{M}_p^T)^{-1} M_p w = M^{-1} M_p w = \rho.$$

3.1. Moore-Penrose stability. Care must be taken in the explicit inverse of $M_p M_p^T$ as it can be singular from, for example, empty rows of M_p if there are no particles in the support of an FE basis function. Defining the particle grid is under the control of the algorithm, unlike in coarse-graining and field solves, and sufficient constraints must be understood. A necessary condition for stability of the pseudoinverses is that there does not exist a set of vertices whose union of support of associated FE basis functions contains less

particles than the number of vertices in the set. This is not rigorous but comes from the intuition that no set of equations (rows of M_p) should have less non-empty columns than rows, otherwise the matrix locally singular. Further we find that more particles than basis functions are required for stability in, for example, the 1D periodic direction if, with degree Q element (e.g., $Q = 2$, a Q2 element), there are Q particles per cell, which results in an equal number of particles and basis functions (equations or vertices). M_p is square in this case, but we observe that $(M_p M_p^T)$ is singular except for the special case where the particles and mesh points are aligned as in the direct remap method in §5. This criterion is not practical to check with an arbitrary set of particles, but we believe that a simple criterion is robust in our experience although not tight. With tensor elements, we use $(Q + 1)^D$ particles per cell.

4. Numerical methods and Landau damping test. Consider the classic one-dimensional plasma test, Landau damping, given by the initial state,

$$(4.1) \quad f(x, v) = \frac{1}{\sqrt{2\pi}} e^{-v^2} (1 + A \cos(kx)),$$

$$(4.2) \quad (x, v) = [0, 2\pi/k] \times [-v_{max}, v_{max}],$$

where $k = 0.5$, $v_{max} = 6$, and we consider three values for the wave amplitude, A : 0.5, 0.01 and 0.0001. The Landau damping test is a popular choice for Vlasov benchmarking because it involves a number of purely kinetic effects, such as phase mixing, and it has simple analytical solutions. A detailed description of the analytical solutions to the Landau damping problem can be found in [13]. To focus on the electrostatic kinetic effects, we ignore collisional dynamics and reduce the full VML equations to the collisionless, magnetic-free Vlasov-Poisson (VP) system.

The two cases where the wave amplitude, A , is 0.01 and 0.5 are referred to as the *linear* and *nonlinear* Landau damping test cases, respectively [21, 9]. A third test case, $A = 0.0001$, sits well within the linear regime and is also common. In the linear case, the small field perturbation is damped out at a rate of $\gamma = -0.153$ in favor of a more homogeneous field. However, in collisionless tests the growth of subgrid modes can disrupt the field damping and cause large gradients to develop in the phase space. These large gradients lead to a sudden regrowth of the field. Previous work [21] has show that the inclusion of collisions can remove these subgrid modes, damping the field to machine precision with a continuum code.

In the nonlinear case, $A = 0.5$, the field decay reverses much earlier and the general dynamics differ from that of the linear case. The two primary explanations for this earlier field resurgence are the stronger interaction between the potential well created by the electric field which resonates with and accelerates more of the particles, and the increased phase mixing, evident in phase-space diagrams. To fully capture these dynamics, the nonlinearized form of the Vlasov equation must be considered. Significant work was done by Villani and Mouhot in [31] to analyze the nonlinear Vlasov equation and show that, while the nonlinear dynamics present in this system lead to a weaker initial decay of the electric field, over long enough time scales, the field will damp out, as it does in the linear case. Thus, it is vital to develop the tools necessary to capture the long time evolution of these kinetic plasmas structures. From [21] and [9], we expect the initial damping rate of the field to be $\gamma_1 = -0.286$ which quickly turns into a field growth at a rate of $\gamma_2 = 0.086$. We will use these values to verify our tests in later sections.

4.1. PETSc test harness. The testing code for this paper is build on the PETSc-PIC framework [13, 35, 36], a recently developed PIC toolkit in the PETSc [6, 11]. The PETSc-PIC framework primarily relies on two modules to drive forward the particle and finite element space. These modules are DMSwarm [30] and DMPLEX [24], respectively. DMSwarm provides a fully parallel solution for particle methods and for particle-mesh methods while DMPLEX provides generic unstructured mesh creation, manipulation and I/O.

The finite element method (FEM) is used to solve the field equations at each timestep. The PETSc FEM framework abstracts the construction of the finite element using the Ciarlet triple [10], consisting of a mesh object (DMPLEX), a finite-dimensional function space (PetscSpace), and a dual space (PetscDualSpace). This is all handled by the PetscFE object and can be customized from the command line. In previous work [13], simple H^1 finite element spaces have been sufficient in capturing the short timescale linear plasma kinetics. Thus, we will continue the use of these H^1 spaces in this work.

Particle pushing for the VP system relies on the characteristics of linear hyperbolic Vlasov equation

which may be derived by first written a simplified form of the Vlasov equation,

$$(4.3) \quad \begin{aligned} \frac{\partial f_\alpha}{\partial t} + \frac{\partial \vec{x}}{\partial t} \cdot \nabla_x f_\alpha + \frac{\partial \vec{v}}{\partial t} \cdot \nabla_v f_\alpha &= 0 \\ \frac{\partial f_\alpha}{\partial t} + \mathbf{z} \cdot \nabla_{\mathbf{q}} f_\alpha &= 0, \end{aligned}$$

where $\mathbf{q} = (\mathbf{x}, \mathbf{v})$ is the phase space variable and $\mathbf{z} = (\mathbf{v}, -q_e \mathbf{E}/m)$ is the combined force. The force term $-q_e \mathbf{E}/m$ is independent of velocity, and therefore (4.3) may be written in the conservative form,

$$(4.4) \quad \frac{\partial f_\alpha}{\partial t} + \nabla_{\mathbf{q}} \cdot (\mathbf{z} f_\alpha) = 0.$$

Given this advective form of the Vlasov equation, we can rewrite the equation for the characteristics $\mathbf{Q} = (\mathbf{X}, \mathbf{V})$,

$$(4.5) \quad \frac{d\mathbf{Q}}{dt} = \mathbf{z},$$

which re-expressed with the original phase-space variables gives,

$$(4.6) \quad \begin{aligned} \frac{d\mathbf{X}}{dt} &= \mathbf{V}, \\ \frac{d\mathbf{V}}{dt} &= -\frac{q_e}{m} \mathbf{E}. \end{aligned}$$

Since particles follow characteristics, the Vlasov equation in the particle basis becomes

$$(4.7) \quad \begin{aligned} \frac{d\mathbf{x}_p}{dt} &= \mathbf{v}_p, \\ \frac{d\mathbf{v}_p}{dt} &= -\frac{q_e}{m} \mathbf{E}. \end{aligned}$$

Solving the characteristic equations is conducted in PETSc with the TS module using explicit symplectic integrators, a subclass of geometric integrators introduced by Ruth in [37]. In general, for PIC models, explicit integrators are not energy conservative and have a tendency to increase total energy over long time scales through “numerical heating”. In previous work [22, 13, 35], however, explicit symplectic integrators have been shown to achieve exact conservation of mass and momentum, as well as a stable approximate conservation of the system energy. The PETSc TS module contains well-tested implementations for first- to fourth-order symplectic integrators. For full Tokamak models and collisional cases, the TS module also contains a variety of implicit time integrators. These include the recently added discrete gradients method which has been tested on both VP and collisional Landau systems [14]. With these implicit methods, larger time steps can be taken while remaining stable, capturing long time physical phenomena. Furthermore, exact energy conservation has been previously shown using implicit methods [29]. In this work, however, we are interested in capturing the fastest waves in the Landau damping system. Thus, explicit methods are more appropriate and less costly than implicit integrators. We choose a first-order symplectic integrator, called *symplectic Euler*.

4.2. Particle grids and finite element order. The phase space continuum grids in this work are on regular 90 degree lattice with an option for simple r-refinement in velocity space. Cartesian sub-particle grids are defined in each phase space cell, similar to Lapenta (Figure 1, [27]). For simplicity, the original grid is used for resampling in this work and adaptivity strategies are left for future work. As discussed in §3.1, with periodic boundary conditions in the spatial dimension and natural boundary conditions in velocity dimension we use at least $Q + 1$ particles in each dimension in each phase space cell for stability of the pseudoinverse.

The test harness is equipped with a simple *r-adaptivity* capability where points are pushed toward the origin in velocity space to better represent a Maxwellian distribution. Figure 1 shows the electric field (E) on uniform and r-refined versions of a 64×128 particle grid $X \times V$, with particle clustering around $v = 0$ and the initial perturbation in x of the electric field. [Data with r-refinement grids have “graded” in the title of the plot and uniform grid data have “uniform” in the title.](#) Similarly, the order of the finite element space in the data is encoded in the title, for example, $Q_x1 - Q_v2$ uses linear $Q1$ (or $P1$) elements in real space and quadratic elements in velocity space.

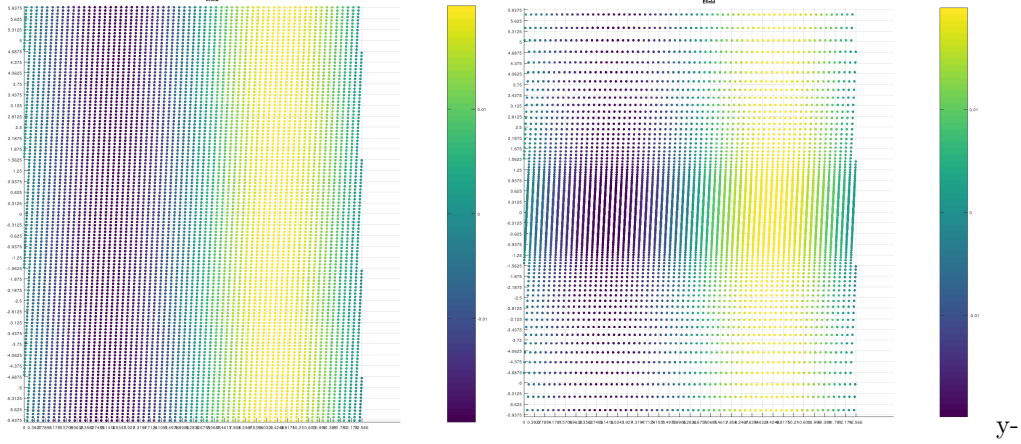


Fig. 1: E field on 64×128 particle grid (y-axis is velocity): uniform distribution (left); r-refinement (right)

5. Finite element version of the direct remap method. Colella et al. developed a method that can be viewed as a version of our algorithm in a finite volume context. In this algorithm continuum space points define the new particle points directly allowing for a trivial map from the grid to particles [43, 32, 33]. That is, $M_p = I$ in (2.3) and the pseudoinverse vanishes. Cubic splines are used for particle deposition on Cartesian grids, demonstrate high-order convergence [32], and use phase-space adaptive mesh refinement (AMR) grids [33]. **This method should conserve energy because the cubic spines can represent a second order polynomial exactly and the direct remap obviously conserves all moments.**

The test harness supports a direct map method in a vertex-centered, finite element context. Linear $Q1$ elements are used in the velocity and space dimension on Cartesian grids. Particles are placed at vertices and the domain is doubly periodic (to make M_p square), which is immaterial given that there should be negligible density at the velocity boundary. The salient feature of this construct is that the particle mass matrix is the identity, $\bar{M}_p = I$, and the pseudoinverse vanishes. These experiments are intended to observe the qualitative effect of high-order grid to particle mapping. Quantitatively, the direct map approach conserve energy to about four digits with $Q1$ in velocity space (see the `src/A.01` directory in the repository). These $Q1$ elements in velocity space with two particles per cell should, in theory conserve momentum only.

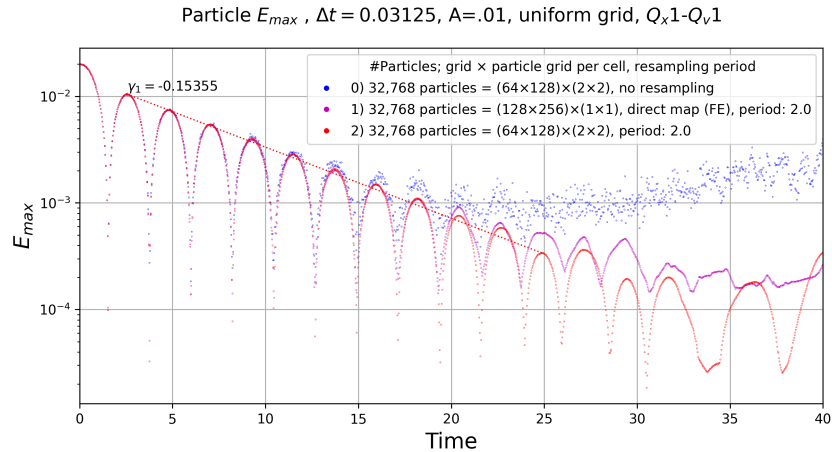


Fig. 2: Particle electric field amplitude linear Landau damping, $A = 0.01$, no resampling (blue and noisy), a direct remapping finite element version of Myers et al. (magenta), and the projection method (red)

Direct map resampling is tested with a linear Landau damping, $A = 0.01$, problem with a 128×256

particle grid and $V_{max} = 6.0$ and results in Figure 2 agree well with amplitude reported in [32] (Figure 3.1). $Q_1 - Q_1$ is used for the projection method with one particle per cell, or vertex, to mimic the direct map method, and the projection method uses a 2×2 particle grid per cell and half as many cells in each dimension to maintain the same number of particles for all three tests and to ensure stability of the pseudo-inverse. This data shows the efficacy of resampling in that it suppresses the noise observed without resampling for the $A = 0.01$ case that was also observed by Colella et al. and some increase in stability is observed with the pseudoinverse technique.

6. Numerical experiments with pseudoinverse resampling. This section investigates this projection resampling method on a linear and a nonlinear Landau damping tests. One issue to be addressed in a PIC method is ensuring a C^0 electric field, which our C^0 discretization of the Poisson equation does not provide given that one order of continuity is lost in the gradient of the potential. One can use an $H(div)$ Poisson solver or C^1 finite elements, but with C^0 elements we project the field to the vertices and then back to the particles, resulting a C^0 electric field. This method helps to stabilize our method, is all but required for $Q2$ elements in space. These instabilities could potentially be addressed with a quite start method [38]. Mesh adaptivity in velocity space [3], may act as a type of quite start, and is a subject of future work.

6.1. Nonlinear Landau damping. The nonlinear Landau damping test case, defined as setting $A = 0.5$, has been studied extensively in the literature (Kraus Table 5.1 tabulates several results of previous work [21]). Cheng and Knorr test with a 32×128 cell continuum grid solver and a time step of $\frac{1}{8}$ that is not only quantitatively similar to our results (Figure 4b) but qualitatively similar (Figure 4 in [9] and Figure 5 in [23] shows γ_1 measured with the first two peaks, and the fourth peak while the third is low). Figure 3 and 4 show convergence studies on the amplitude of the electric field for time step, resampling rate and particle and continuum grid resolution.

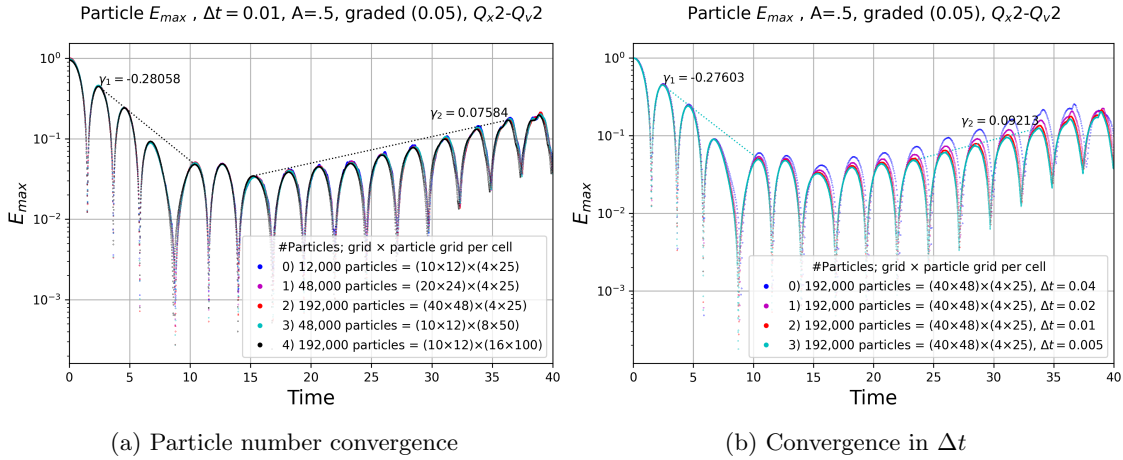


Fig. 3: Converge study of nonlinear Landau damping, $A = 0.5$

These convergence tests establish parameters for an highly resolved analysis in Figure 4b that agrees well with Cheng and Knorr: $\gamma_1 = -0.281$ as compared to our rate of -0.278 , and a growth rate of 0.084 vs our rate of 0.090 . Figure 3b shows convergence study in time step where convergence is observed in the rebound region. The modest effect of resampling in this nonlinear case is observed in Figure 4a, where resampling appears to increase the amplitude in the rebound stage.

6.2. Linear Landau damping. The linear case of Landau damping, $A = 0.0001$, is used here to demonstrate the potential of the projection algorithm. Figure 5 shows the electric field amplitude with a variety of resampling rates with $Q2$ spaces in both real space and velocity space. A damping rate of $\gamma_1 = -0.15348$ is observed, which agrees with theory reported in [21]. With no resampling, the results are clearly very noisy while all of the tests with resampling, regardless of the rate, are free of noise. Resampling

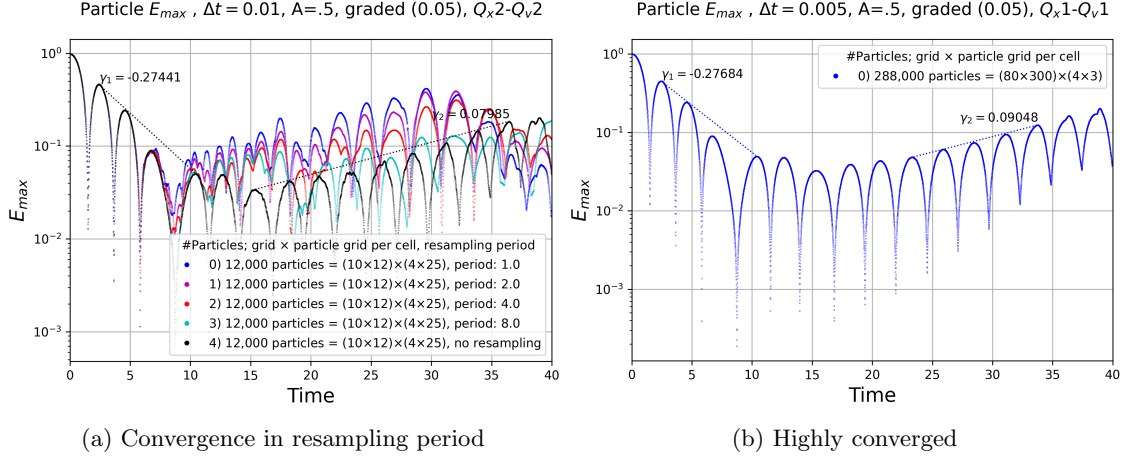


Fig. 4: Converge study of nonlinear Landau damping, $A = 0.5$

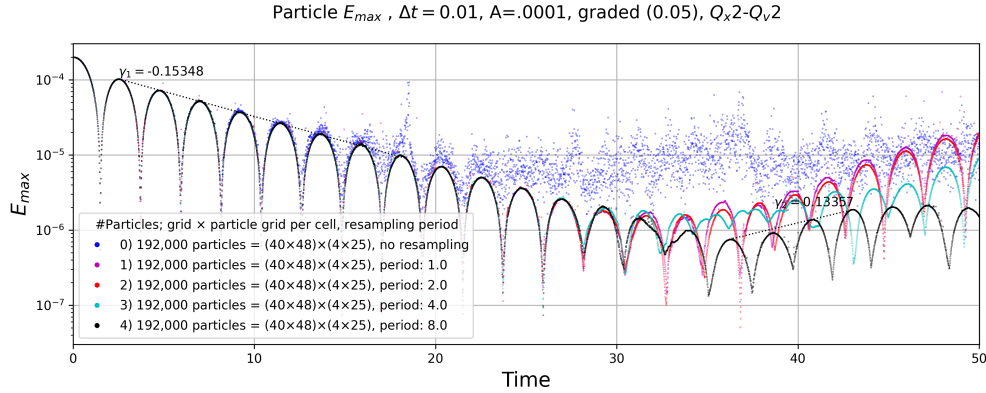


Fig. 5: E_{max} , $A = 0.0001$, resample rate, and without resampling, “convergence” test

does, however, seem to kick the plasma into the growth phase faster, given that tests with a high resampling rate start to grow earlier.

7. Refinement studies and long time stability. In an idealized, infinitely resolved grid, we expect the linear Landau damping problem to decay indefinitely [31]. In a discrete system, however, discretization errors create subgrid modes, with wavelengths bounded by the Nyquist mode, $k_{max} = \pi/\Delta x$. Thus, in coarser grids, high frequency velocity structures in the plasma may *alias* onto lower-wavenumber subgrid modes, which will drive energy back into the field causing the “rebound” effect observed in essentially all collisionless experiments reported in the literature (Fig. 5.3 [21]). This effect can be suppressed by reducing the grid size, Δx , below the Debye length, $\lambda_D = \sqrt{1/n^3}$ in 1D normalized form, where $n = \int_{\Omega} f dv$ is the total plasma density. Previous work [7, 46], has suggested an ideal range for suppressing subgrid modes is $0.15 \leq \lambda_D/\Delta x \leq 1.0$. For our system, at the upper limit of this range ($\lambda_D = \Delta x$), given a density of $n = 4\pi$ and a Debye length of $\lambda_D = 0.022$, the number of grid cells will be 560 cells in space.

Figure 6 shows a refinement study in the number of particles per cell which does not effect the location of the rebound. We further note that the level of the rebound converges at about $1M$ particles as is shown in Figure 8b and Figure 6 box “(b)”. The amplitude of the second rebound ($T = 100$ in units of inverse plasma frequency $[\omega_p^{-1}]$) is very close for all but the lowest particle count ($16K$) model and this alternating pattern slowly decays leaving coherent and noise-free waves (see detail at $T = 500$ Figure 8c). However, the $16K$ particle model starts to heat up and continues to grow at longer times ($T = 1,000$ data is available

in the repository). The 65K and 259K models remain stable with clean oscillations up to $T = 1,000$. The observed change in amplitude of the rebound may be explained by the plasma's increased ability to absorb wave energy as the particle density is increased. We expect this to converge monotonically but the additional presence of statistical noise in the system, as well as the rebound's apparent dependence on its state just before rebounding may offer an explanation as to why we do not observe a clean convergence structure.

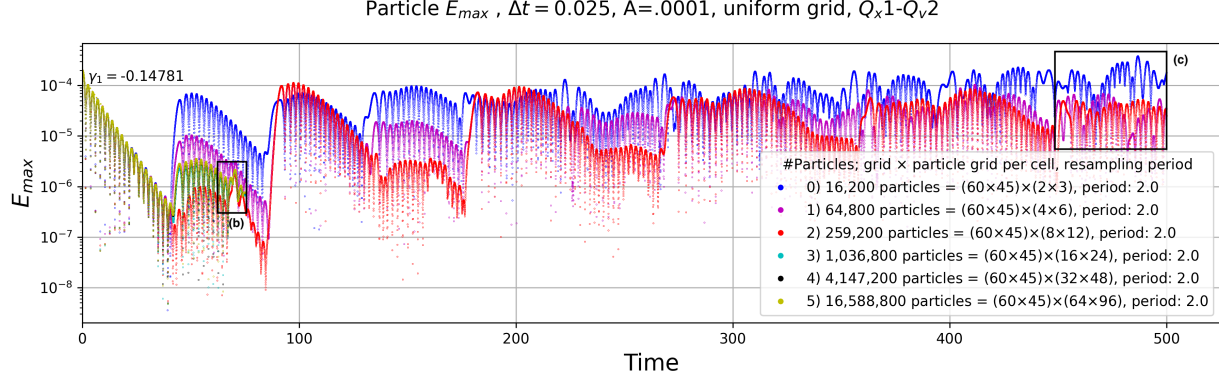


Fig. 6: E_{max} , $A = 0.0001$, Refinement in particles per cell long time simulations

Figure 7 shows refinement studies in grid density with constant number of particles per phase-space cell. An increase in cell count delays the onset of subgrid modes and suppresses the rebound with the largest case almost entirely suppressed before $T = 500$, when a large amplitude subgrid mode erupts and the continues with high-frequency, yet coherent, oscillations.

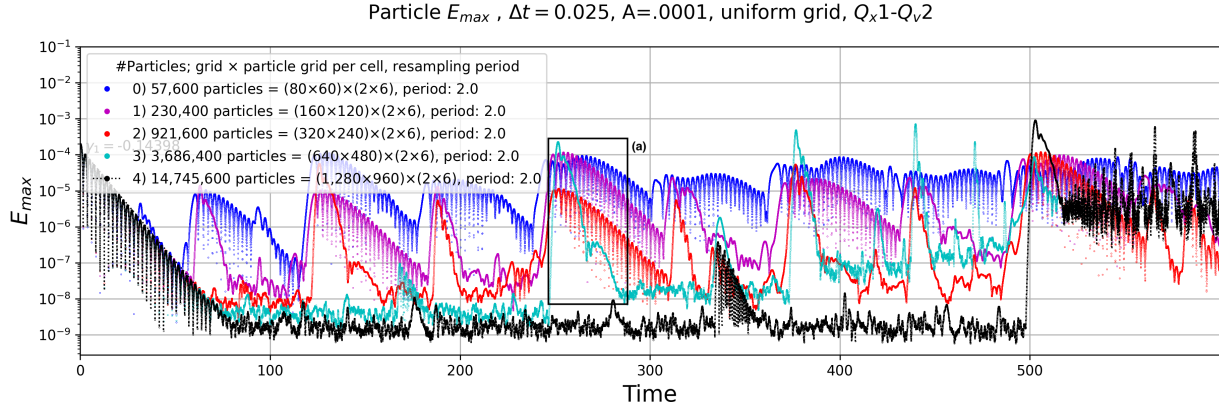


Fig. 7: E_{max} , $A = 0.0001$, Refinement in grid density long time simulations

The choice in timestep is based on previous works with PETSc-PIC [13, 14] and Figure 8a shows little difference with a smaller time step than used in these studies.

8. Side effects of resampling. Figure 4a demonstrates that the dynamics of the plasma is not highly sensitive to the resampling period within a broad range (eg, $1 - 8 [\omega_p^{-1}]$), but that rebound starts a little earlier with higher resampling rates indicating that resampling is disturbing the plasma to some extent. To investigate this effect, Figure 9 (left) shows a linear example with resampling every time step and increasing resampling periods. The highest resampling rates clearly lead to instabilities and these instabilities demonstrate classic growing oscillations up to a small amplitude, see detail in Figure 9 (right), that is growing in mean value and plateaus at about 1.0. Perhaps stability analysis could provide insight on this issue.

While this instability at high resampling rates is not a practical problem, per se, in that all of our tests are stabilized with much lower resampling frequencies, this data does indicate that resampling can

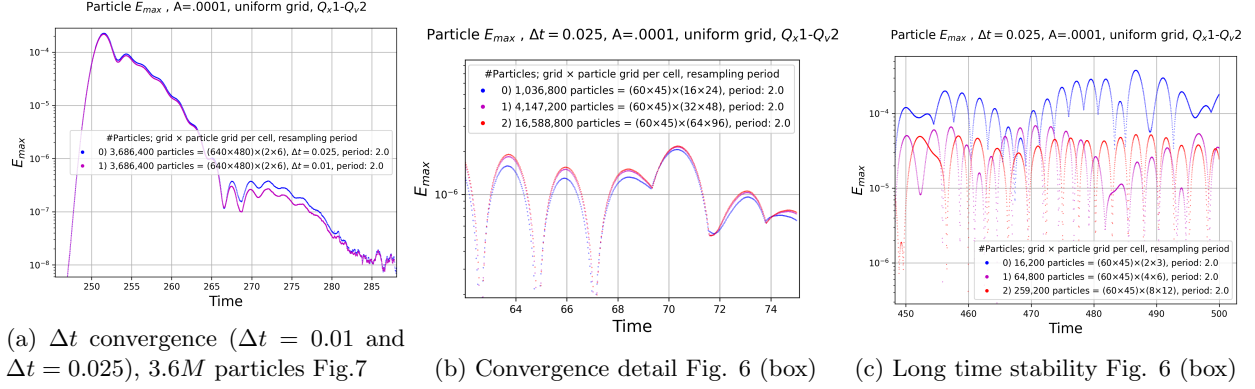


Fig. 8: E_{max} , $A = 0.0001$, long time simulations

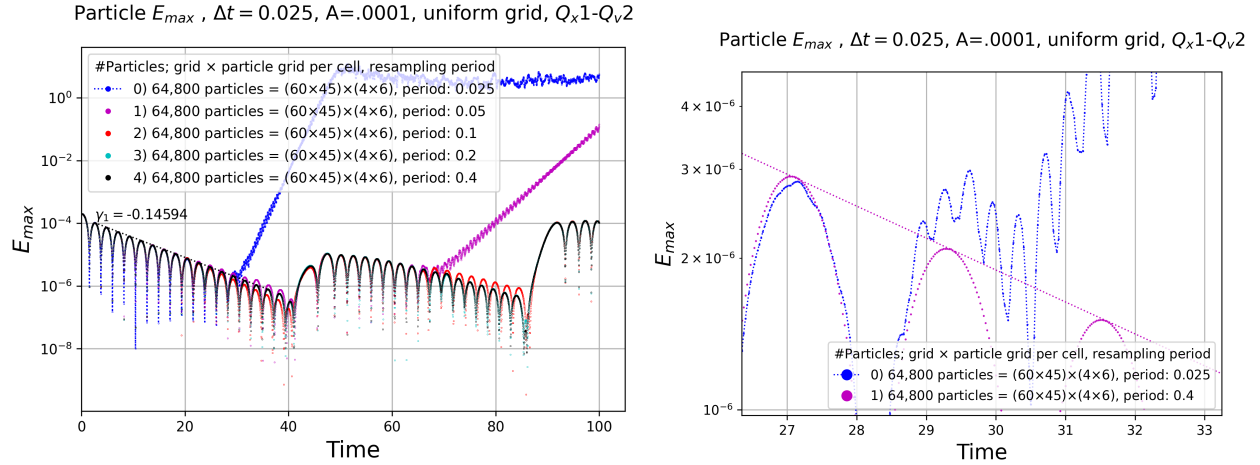


Fig. 9: E_{max} , $A = 0.0001$, resampling period "anti-convergence" study (left), instability detail (right)

have adverse effects. This test problem is highly idealized and does not provide convincing experimental evidence that the adaptivity strategy of simply mapping make to the original grid will be robust in practice. More sophisticated adaptivity strategies are the subject of future work and would require more scientifically relevant models such as problems in magnetic reconnection in at least $2X + 3V$.

8.1. Discussion. Figure 7 sheds light onto the complex relationship and dependency between all the simulation variables, i.e. resampling rate, spatial and velocity grid density and time step. It is difficult to draw definitive conclusions about what exactly is driving the dynamics of the electric field damping and rebounding. As discussed in §7, the grid resolution plays a large role in reducing the interaction of subgrid modes with the physical waves, while the particle density reduces stochastic, noise-driven heating effects in the plasma. These effects do not, however, converge monotonically suggesting that they are linked in some way. This requires further study in future work.

The inclusion of collisions may also provide a smooth mechanism. The collision operator acts as a controlled, physically motivated diffusion term in the kinetic equations. This diffusive term continuously smooths out any build up of high-frequency components in the distribution function which can lead to spurious rebounds. In other algorithms (Fig. 5.5 [21]), clean decays to machine precision have been shown using collisions. Collisions must be used with some level of caution, however. Much of the essential collisionless interactions in the Landau damping test, in particular in the nonlinear regime, rely on fine-scale interactions between the particles and waves. Introducing a collision operator can have the effect of smoothing out those

essential fine-scale interactions which, if too strong, will disrupt the fundamental physics of the system. Recent work in the PETSc library [2, 35, 1, 3] has provided a variety of collision algorithms that can be included in the PETSc-PIC framework in future work. Other methods, such as [47], have reported clean decay without collisions, but the details of the numerical method are not entirely clear and some form of dissipation may be present.

9. Conclusion. The paper develops a new approach to particle resampling that uses a conservative projection, a pseudoinverse, to map any distribution of particles to essentially any other distribution of particle while conserving all moments up to the degree of polynomial that the projection function space can represent exactly. This method is evaluated with a static particle and continuum Cartesian grids, simply remapping to the original particle grid, on standard Landau damping test problems. Tests where noise is problematic, the linear cases, show that resampling reduces noise considerably and coherent dynamics are maintained for long times, where as the solution becomes essentially all noise without resampling.

This work suggests several areas of future work, namely:

Adaptivity strategies. Developing strategies to optimize the particle grids with respect to minimizing disturbances to the physics from resampling.

Entropy. With entropy measures, from our particle Landau collision operator [35], we can determine the continuum grids required for resampling or a continuum collision operator [3, 35] to keep entropy generation by the projection well below the entropy generated by the physics.

Continuum grid AMR. AMR in velocity and regular particle grids on each cell of an adapted grid, like a cubed sphere [3], is a path for generating adapted particle grids through continuum mesh adaptation.

Splitting and coalescing. These ideas, developed in many particle resampling methods, would allow for an incremental modification of the particle mesh to minimize cost and perhaps have less impact the dynamics.

Increasing relevance. Understanding the effects of resampling on physics, beyond conserving moments and other structure like entropy stability, requires experimentation with more complex models such as the Ion Temperature Gradient (ITG) instability to understand the robustness of these ideas.

Acknowledgments. This work was supported by the U.S. Department of Energy, Office of Science, Office of Fusion Energy Sciences and Office of Advanced Scientific Computing Research, Scientific Discovery through Advanced Computing (SciDAC) Partnership programs under Contract No. DE-AC02-05CH11231 at Lawrence Berkeley National Laboratory, the Office of Naval Research and by an appointment to the NRC Research Associateship Program at the U.S. Naval Research Laboratory, administered by the Fellowships Office of the National Academies of Sciences, Engineering, and Medicine. DSF and MGK were partially supported by NSF CSSI grant 1931524.

Appendix A. Artifact description and reproducibility.

PETSc output files with all data, provenance information, and reproducibility instructions for all tables and plots can be obtained from `git@gitlab.com:markadams4/resampling-paper.git`. This includes the python scrips that generates the plots and run scripts, makefiles and PETSc resource files used to generate the data, and the test harness code in `src`. The `src/A.X` directories has data for $A = 0.X$. The exact PETSc versions (SHA1) are in the data files, with the provenance data, all parameters used in each test, but any PETSc version from v3.22 should suffice to reproduce this data.

REFERENCES

- [1] M. F. ADAMS, D. P. BRENNAN, M. G. KNEPLEY, AND P. WANG, *Landau collision operator in the CUDA programming model applied to thermal quench plasmas*, in 2022 IEEE International Parallel and Distributed Processing Symposium (IPDPS), 2022, pp. 115–123, <https://doi.org/10.1109/IPDPS53621.2022.00020>.
- [2] M. F. ADAMS, E. HIRVIJOKI, M. G. KNEPLEY, J. BROWN, T. ISAAC, AND R. MILLS, *Landau collision integral solver with adaptive mesh refinement on emerging architectures*, SIAM Journal on Scientific Computing, 39 (2017), pp. C452–C465, <https://doi.org/10.1137/17M1118828>, <http://epubs.siam.org/doi/abs/10.1137/17M1118828>, <https://arxiv.org/abs/1702.08880>.
- [3] M. F. ADAMS, P. WANG, J. MERSON, K. HUCK, AND M. G. KNEPLEY, *A performance portable, fully implicit landau collision operator with batched linear solvers*, SIAM Journal on Scientific Computing, 47 (2025), pp. B360–B381, <https://doi.org/10.1137/24M1640252>, <https://doi.org/10.1137/24M1640252>, <https://arxiv.org/abs/https://doi.org/10.1137/24M1640252>.
- [4] C. L. AND, *On self-similar collapsing solutions to the kinetic equations of stellar dynamics*, Transport Theory and Statistical Physics, 36 (2007), pp. 281–297, <https://doi.org/10.1080/00411450701465676>.

- [5] F. ASSOUS, T. POUGEARD DULIMBERT, AND J. SEGRA, *A new method for coalescing particles in PIC codes*, Journal of Computational Physics, 187 (2003), pp. 550–571, [https://doi.org/10.1016/S0021-9991\(03\)00124-4](https://doi.org/10.1016/S0021-9991(03)00124-4).
- [6] S. BALAY, S. ABHYANKAR, M. F. ADAMS, S. BENSON, J. BROWN, P. BRUNE, K. BUSCHELMAN, E. M. CONSTANTINESCU, L. DALCIN, A. DENER, V. ELJKHOUT, J. FAIBUSSOWITSCH, W. D. GROPP, V. HAPLA, T. ISAAC, P. JOLIVET, D. KARPEEV, D. KAUSHIK, M. G. KNEPLEY, F. KONG, S. KRUGER, D. A. MAY, L. C. MCINNES, R. T. MILLS, L. MITCHELL, T. MUNSON, J. E. ROMAN, K. RUPP, P. SANAN, J. SARICH, B. F. SMITH, S. ZAMPINI, H. ZHANG, H. ZHANG, AND J. ZHANG, *PETSc Web page*. <https://petsc.org/>, 2022, <https://petsc.org/>.
- [7] C. K. BIRDSALL AND N. MARON, *Plasma self-heating and saturation due to numerical instabilities*, Journal of Computational Physics, 36 (1980), pp. 1–19, [https://doi.org/https://doi.org/10.1016/0021-9991\(80\)90171-0](https://doi.org/https://doi.org/10.1016/0021-9991(80)90171-0), <https://www.sciencedirect.com/science/article/pii/0021999180901710>.
- [8] Y. CHEN AND S. E. PARKER, *Coarse-graining phase space in δf particle-in-cell simulations*, Physics of Plasmas, 14 (2007), p. 082301, <https://doi.org/10.1063/1.2751603>, <https://doi.org/10.1063/1.2751603>, <https://arxiv.org/abs/https://doi.org/10.1063/1.2751603>.
- [9] C. CHENG AND G. KNORR, *The integration of the Vlasov equation in configuration space*, Journal of Computational Physics, 22 (1976), pp. 330–351, [https://doi.org/https://doi.org/10.1016/0021-9991\(76\)90053-X](https://doi.org/https://doi.org/10.1016/0021-9991(76)90053-X), <https://www.sciencedirect.com/science/article/pii/002199917690053X>.
- [10] P. G. CIARLET, *Numerical Analysis of the Finite Element method*, Les Presses de L'Université de Montréal, 1976.
- [11] S. B. ET. AL., *PETSc/TAO Users Manual*, Argonne National Laboratory, 2022.
- [12] D. FAGHIHI, V. CAREY, C. MICHOSKI, R. HAGER, S. JANHUNEN, C. CHANG, AND R. MOSER, *Moment preserving constrained resampling with applications to particle-in-cell methods*, Journal of Computational Physics, 409 (2020), p. 109317, <https://doi.org/https://doi.org/10.1016/j.jcp.2020.109317>, <https://www.sciencedirect.com/science/article/pii/S0021999120300917>.
- [13] D. S. FINN, M. G. KNEPLEY, J. V. PUSZTAY, AND M. F. ADAMS, *A numerical study of landau damping with petsc-pic*, Communications in Applied Mathematics and Computational Science, 18 (2023), p. 135–152, <https://doi.org/10.2140/camcos.2023.18.135>, <http://dx.doi.org/10.2140/camcos.2023.18.135>.
- [14] D. S. FINN, J. V. PUSZTAY, M. G. KNEPLEY, AND M. F. ADAMS, *Entropy monotonicity using discrete gradients in the vlasov-poisson-landau system*, Submitted to Journal of Computational Physics, (2025).
- [15] A. GONOSKOV, *Agnostic conservative down-sampling for optimizing statistical representations and pic simulations*, Computer Physics Communications, 271 (2022), p. 108200, <https://doi.org/https://doi.org/10.1016/j.cpc.2021.108200>, <https://www.sciencedirect.com/science/article/pii/S001046552100312X>.
- [16] R. HAZELTINE AND J. MEISS, *Plasma Confinement*, Dover Books on Physics, Dover Publications, 2013, <https://books.google.com/books?id=LDPDAgAAQBAJ>.
- [17] E. HIRVIOKI, *Structure-preserving marker-particle discretizations of Coulomb collisions for particle-in-cell codes*, Plasma Physics and Controlled Fusion, 63 (2021), p. 044003, <https://doi.org/10.1088/1361-6587/abe884>, <https://doi.org/10.1088/1361-6587/abe884>.
- [18] E. HIRVIOKI AND M. F. ADAMS, *Conservative discretization of the Landau collision integral*, Physics of Plasmas, 24 (2017), p. 032121, <https://doi.org/10.1063/1.4979122>, <http://dx.doi.org/10.1063/1.4979122>, <https://arxiv.org/abs/http://dx.doi.org/10.1063/1.4979122>.
- [19] E. HIRVIOKI, M. KRAUS, AND J. W. BURBY, *Metriplectic particle-in-cell integrators for the landau collision operator*, 2018, <https://arxiv.org/abs/1802.05263>, <https://arxiv.org/abs/1802.05263>.
- [20] P. KILIAN, V. ROYTERTSHEYN, AND J. SCUDDER, *The Role of Coulomb Collisions and Large-Scale Electric Field in Shaping Electron Velocity Distributions in the Solar Wind*, in APS Division of Plasma Physics Meeting Abstracts, vol. 2021 of APS Meeting Abstracts, Jan. 2021, p. UP11.078.
- [21] M. KRAUS, *Variational integrators in plasma physics*, 2014, <https://arxiv.org/abs/1307.5665>, <https://arxiv.org/abs/1307.5665>.
- [22] M. KRAUS AND E. HIRVIOKI, *Metriplectic integrators for the Landau collision operator*, Physics of Plasmas, 24 (2017), <https://doi.org/10.1063/1.4998610>.
- [23] M. KRAUS, K. KORMANN, J. MORRISON, PHILIP, AND E. SONNENDRÜCKER, *Gempic: geometric electromagnetic particle-in-cell methods*, Journal of Plasma Physics, 83 (2017), p. 905830401, <https://doi.org/10.1017/S002237781700040X>.
- [24] M. LANGE, L. MITCHELL, M. G. KNEPLEY, AND G. J. GORMAN, *Efficient mesh management in Firedrake using PETSc-DMplex*, SIAM Journal on Scientific Computing, 38 (2016), pp. S143–S155, <https://doi.org/10.1137/15M1026092>, <https://arxiv.org/abs/http://arxiv.org/abs/1506.07749>.
- [25] G. LAPENTA, *Particle rezoning for multidimensional kinetic particle-in-cell simulations*, Journal of Computational Physics, 181 (2002), pp. 317–337, <https://doi.org/10.1006/jcph.2002.7126>.
- [26] G. LAPENTA AND J. BRACKBILL, *Dynamic and selective control of the number of particles in kinetic plasma simulations*, Journal of Computational Physics, 115 (1994), pp. 213–227, <https://doi.org/10.1006/jcph.1994.1188>.
- [27] G. LAPENTA AND J. BRACKBILL, *Control of the number of particles in fluid and mhd particle in cell methods*, Computer Physics Communications, 87 (1995), pp. 139–154, [https://doi.org/10.1016/0010-4655\(94\)00180-A](https://doi.org/10.1016/0010-4655(94)00180-A).
- [28] P. LUU, T. TÄCKELMANTEL, AND A. PUKHOV, *Voronoi particle merging algorithm for pic codes*, Computer Physics Communications, 202 (2016), pp. 165–174, <https://doi.org/10.1016/j.cpc.2016.01.009>.
- [29] S. MARKIDIS AND G. LAPENTA, *The energy conserving particle-in-cell method*, Journal of Computational Physics, 230 (2011), pp. 7037–7052, <https://doi.org/https://doi.org/10.1016/j.jcp.2011.05.033>, <https://www.sciencedirect.com/science/article/pii/S0021999111003445>.
- [30] D. A. MAY AND M. G. KNEPLEY, *DMSwarm: Particles in PETSc*, in EGU General Assembly Conference Abstracts, vol. 19, 2017, p. 10133.
- [31] C. MOUHOT AND C. VILLANI, *On Landau Damping*, Acta Mathematica, 207 (2011), pp. 29 – 201, <https://doi.org/10.1007/s11511-011-0068-9>, <https://doi.org/10.1007/s11511-011-0068-9>.
- [32] A. MYERS, P. COLELLA, AND B. V. STRAALEN, *A 4th-order particle-in-cell method with phase-space remapping for the*

- Vlasov–Poisson equation*, SIAM Journal on Scientific Computing, 39 (2017), pp. B467–B485, <https://doi.org/10.1137/16M105962X>, <https://arxiv.org/abs/https://doi.org/10.1137/16M105962X>.
- [33] A. MYERS, P. COLELLA, AND B. VAN STRAALLEN, *The convergence of particle-in-cell schemes for cosmological dark matter simulations*, The Astrophysical Journal (Online), 816 (2016), <https://doi.org/10.3847/0004-637X/816/2/56>, <https://www.osti.gov/biblio/1525130>.
 - [34] M. PFEIFFER, A. MIRZA, C.-D. MUNZ, AND S. FASOULAS, *Two statistical particle split and merge methods for particle-in-cell codes*, Computer Physics Communications, 191 (2015), pp. 9–24, <https://doi.org/https://doi.org/10.1016/j.cpc.2015.01.010>, <https://www.sciencedirect.com/science/article/pii/S0010465515000302>.
 - [35] J. PUSZTAY, F. ZONTA, M. KNEPLEY, AND M. ADAMS, *The Landau collision integral in the particle basis in the PETSc library*, 2023, <https://arxiv.org/abs/2306.12606>.
 - [36] J. V. PUSZTAY, M. G. KNEPLEY, AND M. F. ADAMS, *Conservative projection between finite element and particle bases*, SIAM Journal on Scientific Computing, 44 (2022), pp. C310–C319, <https://doi.org/10.1137/21M1454079>, <https://doi.org/10.1137/21M1454079>, <https://arxiv.org/abs/https://doi.org/10.1137/21M1454079>.
 - [37] R. D. RUTH, *A Canonical Integration Technique*, IEEE Transactions on Nuclear Science, 30 (1983), p. 2669, <https://doi.org/10.1109/TNS.1983.4332919>.
 - [38] R. SYDORA, *Low-noise electromagnetic and relativistic particle-in-cell plasma simulation models*, Journal of Computational and Applied Mathematics, 109 (1999), pp. 243–259, [https://doi.org/https://doi.org/10.1016/S0377-0427\(99\)00161-2](https://doi.org/https://doi.org/10.1016/S0377-0427(99)00161-2), <https://www.sciencedirect.com/science/article/pii/S0377042799001612>.
 - [39] J. TEUNISSEN AND U. EBERT, *Controlling the weights of simulation particles: Adaptive particle management using k-d trees*, Journal of Computational Physics, 259 (2014), pp. 318–330, <https://doi.org/10.1016/j.jcp.2013.12.005>.
 - [40] T. VERNAY, S. BRUNNER, L. VILLARD, B. F. MCMILLAN, S. JOLLIET, T. M. TRAN, AND A. BOTTINO, *Synergy between ion temperature gradient turbulence and neoclassical processes in global gyrokinetic particle-in-cell simulations*, Physics of Plasmas, 19 (2012), p. 042301, <https://doi.org/10.1063/1.3699189>, <https://doi.org/10.1063/1.3699189>, <https://arxiv.org/abs/https://pubs.aip.org/aip/pop/article-pdf/doi/10.1063/1.3699189/13641048/042301.1.online.pdf>.
 - [41] C. VOCKS, *A kinetic model for ions in the solar corona including wave-particle interactions and coulomb collisions*, The Astrophysical Journal, 568 (2002), p. 1017, <https://doi.org/10.1086/338884>, <https://dx.doi.org/10.1086/338884>.
 - [42] M. VRANIC, T. GRISMAYER, J. MARTINS, R. FONSECA, AND L. SILVA, *Particle merging algorithm for pic codes*, Computer Physics Communications, 191 (2015), pp. 65–73, <https://doi.org/10.1016/j.cpc.2015.01.020>.
 - [43] B. WANG, G. H. MILLER, AND P. COLELLA, *A particle-in-cell method with adaptive phase-space remapping for kinetic plasmas*, SIAM Journal on Scientific Computing, 33 (2011), pp. 3509–3537, <https://doi.org/10.1137/100811805>, <https://doi.org/10.1137/100811805>, <https://arxiv.org/abs/https://doi.org/10.1137/100811805>.
 - [44] A. WEINSTEIN AND P. J. MORRISON, *Comments on: The Maxwell-Vlasov equations as a continuous Hamiltonian system*, Physics Letters A, 86 (1981), pp. 235–236, [https://doi.org/https://doi.org/10.1016/0375-9601\(81\)90496-5](https://doi.org/https://doi.org/10.1016/0375-9601(81)90496-5), <https://www.sciencedirect.com/science/article/pii/0375960181904965>.
 - [45] D. WELCH, T. GENONI, R. CLARK, AND D. ROSE, *Adaptive particle management in a particle-in-cell code*, Journal of Computational Physics, 227 (2007), pp. 143–155, <https://doi.org/10.1016/j.jcp.2007.07.015>.
 - [46] G. WERNER, L. ADAMS, AND J. CARY, *Suppressing grid instability and noise in particle-in-cell simulation by smoothing*, 03 2025, <https://doi.org/10.48550/arXiv.2503.05123>.
 - [47] T. ZHOU, Y. GUO, AND C.-W. SHU, *Numerical study on Landau damping*, Physica D Nonlinear Phenomena, 157 (2001), pp. 322–333, [https://doi.org/10.1016/S0167-2789\(01\)00289-5](https://doi.org/10.1016/S0167-2789(01)00289-5).